Journal of Electroanalytical Chemistry 799 (2017) 487–496

Contents lists available at ScienceDirect

Journal of Electroanalytical Chemistry

journal homepage: www.elsevier.com/locate/jelechem

Differentiated interactions in phosphate solutions: Comparing Ag(111) and Ag(100) surfaces

Claudia B. Salim Rosales[a], Mariana I. Rojas[b,*], Lucía B. Avalle[c,*]

[a] Grupo de Electroquímica Experimental y Teórico. Instituto de Física Enrique Gaviola (IFEG), Consejo Nacional de Investigaciones Científicas y Técnicas (CONICET), Argentina

[b] INFIQC, Departamento de Matemática y Física, Facultad de Ciencias Químicas, Universidad Nacional de Córdoba, Ciudad Universitaria, Córdoba 5000, Argentina

[c] Facultad de Ciencias Exactas y Naturales, Universidad Nacional de Catamarca Consejo Nacional de Investigaciones Científicas y Técnicas (CONICET), Argentina

ARTICLE INFO

Keywords:
Ag(111)
Ag(100)
Phosphates
Cyclic voltammetry
DFT

ABSTRACT

The electrochemical behavior of phosphate species on Ag(111) and Ag(100) single crystal surfaces was studied by experimental techniques and theoretical calculations. Characteristic cathodic/anodic potential peaks (V_p) appear in the current density-potential curves (*j–V*) for $H_2PO_4^-$, H_3PO_4, and in the case of PO_4^{3-} for concentrations lower than 0.1 M, where the interaction is stronger for the Ag(100) electrode. This demonstrate that the adsorption is sensitive to the surface structure. The adsorption energy (E_{ads}) of the different species on both surfaces was studied by means of DFT-vdW calculations. All phosphate species have tri-dentate binding. The $|E_{ads}|$ increased for the H_3PO_4; $H_2PO_4^-$; HPO_4^{2-} and PO_4^{3-} sequence, and the tetrahedral structures are compressed. Although the same trend was observed on both crystalline surfaces, the films have the symmetry of the substrate, C_{3v} and C_{4v}. The influence of hydroxide co-adsorption was studied for different $[HPO_4^{2-}]/[PO_4^{3-}]$ ratios in solution. The strength of adsorption obtained from experimental and theoretical calculations show an excellent qualitative correlation.

1. Introduction

Phosphate adsorption on single crystal surfaces of metals has been reported for different electrolytes [1-3,5-18]. While specific adsorption occurs below the *pztc*, desorption takes place at potentials above the *pztc*, depending on the surface. The controversy found in the literature about the interaction between phosphate species and different single crystals, specifically the platinum surface [5,8], can be mainly attributed to the polyprotic nature of phosphoric acid and the inherent complexity of the solid surfaces in contact with the electrolyte, which further complicates its study.

Yaguchi et al. [2] investigated the geometry and nature of phosphate species adsorbed on Au(111) by surface-enhanced infrared absorption spectroscopy in the ATR configuration (ATR-SEIRAS) and DFT calculations. Based on the SEIRA spectra of phosphate species adsorbed on an Au thin-film electrode in 0.1 M phosphate buffer at two different pHs, they have demonstrated that the acid-base equilibrium of adsorbed phosphate species is significantly shifted to lower pH compared to that of phosphate anions in the bulk solution. They postulated, supported by additional information from DFT calculations, that the observed P–O stretching bands corresponded to tri-dentate binding of $(HPO_4)_{ads}$ or $(PO_4)_{ads}$ species, bonded via three oxygen atoms on Au (111) electrode surface. This research represented an important advancement on the identification of surface phosphate species and their dependence on electrode potential and pH. However, an approach that considers the role of solvent and its incidence on the interactions between the crystallographic phase of the electrode and the adsorbed molecule is an issue that is still poorly understood. An advance in this direction can be found in recent research by the F. Tielens group [20].

Surface-Enhanced Raman Spectroscopy (SERS) studies, have shown difficulty in assigning signal shifts to the results from single crystals [19]. This technique has significant restrictions to get a measurable signal/noise ratio, where a surface with a large roughness factor is needed. The recently developed shell-isolated nanoparticle-enhanced Raman spectroscopy (SHINERS) technique [21] allows studying single crystal surfaces in an electrochemical environment. Using an electrochemical in-situ experimental setup (EC-SHINERS) [22,23], the characterization of the adlayer geometries and the detection of intermediate reactive species (likely to have formed during the chemical reactions occurring at the electrode surface) are possible [22,24]. Weber et al. [12] informed that phosphate species adsorption is not sensitive to Pt surface geometry. They reported that the $H_2PO_4^-$ ion was adsorbed in

* Corresponding authors.
E-mail addresses: mrojas@fcq.unc.edu.ar (M.I. Rojas), avalle@famaf.unc.edu.ar (L.B. Avalle).

http://dx.doi.org/10.1016/j.jelechem.2017.06.056
Received 15 January 2017; Received in revised form 29 April 2017; Accepted 28 June 2017
Available online 03 July 2017
1572-6657/

the low potential region, whereas both $H_2PO_4^-$ and HPO_4^{2-} were adsorbed at higher potentials, in contrast with the results obtained by Nikolic et al. [25]. Atomic scale information on electrochemical interfaces has been provided employing single crystals with different crystallographic orientations. Examples can be found in both theoretical and experimental studies. The adsorption of ions on low-index crystal faces of gold, silver and platinum [26–29] is also extended to high-index to systematically study adsorption as well as charge transfer processes. The double layer at the electrode/electrolyte interface is determined by the properties of the metal and the nature of the ions present in the electrolyte [30]. Knowledge of the interactions between the different adsorbed phosphate species and the electrode surface is significant from a biochemical point of view. For example, the charged electrochemical interface can serve as a useful model system for better understanding of the interactions of the phosphate group in biomacromolecules [31,32].

The symmetry of the anion-cluster system and the charge transferred to the metal have been investigated by many authors [33,34]. Anion binding energies, adsorption sites, and adsorbate orientation have been informed for SO_4^{2-}, HSO_4^-, CO_3^{2-}, HCO_3^-, ClO_4^-, NO_3^-, and PO_4^{3-}. Ab-initio quantum mechanical calculations were used to study low-index single crystal silver surfaces. It was observed that the binding energies for different coordinations of phosphate anions increased from mono-dentate, bi-dentate and tri-dentate, and comparable binding energies values on the (111) and (100) crystal faces were reported [33].

In the present, work we have performed *j–V* and current transient profiles of Ag(111) and Ag(100) electrodes in K_3PO_4, KH_2PO_4 and H_3PO_4 solutions. In order to take a microscopic view of the adsorption phenomenon, the adsorption process of these species on both surfaces was modeled by means of DFT-vdW calculations. The particular case of $H_2PO_4^-$ ion on Ag (100) surface was explored for three conformations: mono-dentate, bi-dentate or tri-dentate binding. For both surfaces, considering tri-dentate binding, we calculate the PO_4^{3-}, HPO_4^{2-}, $H_2PO_4^-$ and H_3PO_4 adsorption energies, charge transfer process and the change on the geometries. Finally, we analyze the experimental and theoretical trends.

2. Experimental

2.1. Methods and materials

The working electrodes were Ag(hkl) single crystals provided by Mateck (orientation accuracy < 1 °). Pretreatment of the crystals was performed by following the same sequence of steps before the beginning of each measurement as in Refs. [32,35,36]. The potential of zero charge (*pzc*) of the crystallographic orientation of the electrode surface was measured in 0.010 M $KClO_4$ by electrochemical Impedance Spectroscopy (EIS) and values of -0.735 V and -0.865 V vs. SCE were obtained for Ag(111) and Ag(100) electrodes, respectively [35,37]. Oxygen free solutions were obtained by continuously purging the electrochemical cell with nitrogen gas (99.999% purity). Water from a Milli-Q Millipore System was used for the preparation of all solutions and also for glassware cleaning. Some of the phosphate solutions studied were prepared from recrystallized salts such as KH_2PO_4. All chemicals were of analytical grade. Table 1 shows the calculated concentrations of phosphate species, using published pK_a values. The activity coefficients were taken as unitary.

2.2. Cyclic voltammetry(CV) measurements

The electrochemical analyzer was an AUTOLAB-PGSTAT302N equipped with staircase scan module. The data were collected and analyzed by NOVA 1.7 software. The single crystal electrodes were transferred with a drop of ultrapure water to the electrochemical cell. The contact between the electrode surface and the solution was made by means of the hanging meniscus method under potential control, at a potential below the potential of zero charge. Electrodes treated with this procedure yield nearly ideal voltammetric responses for the underpotential deposition of Pb monolayers according to the literature [38]. Before each measurement, the surface was stabilized by maintaining the potential several minutes at -1.1 V vs. SCE and then cycling in the range of -1.1 V to -0.70 V vs. SCE at 0.050 V/s. The effect of double-layer charging was assessed by subtracting a given baseline from each steady state current voltammogram. Different scan rates were measured to study voltammperometric peaks dependence on potential from 0.010 V s^{-1} to1.0 V s^{-1}.

2.3. Potential step measurements

The current transients were recorded applying a consecutive potential step procedure. Stabilization of the system was performed applying an initial potential, V_i, of -0.40 V. Then, a potential step was applied at a more negative potential value, V_{trans}, and the current was recorded as a function of time. After that, the potential was returned to the initial value.

2.4. Theoretical calculations

Theoretical calculations were performed using SIESTA code (at DFT level with Van der Waals interactions, vdW-DFT) [39]. The silver single crystal surfaces were represented by four sixteen-atom layers and 3D periodic boundary conditions. The optimized lattice parameter for the FCC latice was 4.10 Å. The unit cells were (11.61 Å × 11.61 Å × 30 Å) in both cases; the (100) was orthorhombic and the (111) was hexahedral. Since we are modelling the solid/vacuum interphase, we have chosen a big modulus unit cell vector in the z direction, so the interactions between the system and their images become negligible. We have performed such calculations for different surface dimensions of the unit cell. The optimal super-cell must have low interactions between phosphate species and a reasonable number of atoms to demand an affordable computational cost. We have chosen (4 × 4) because it was found to be more adequate for the present purpose. To model the interaction between the adsorbed phosphate species at low coverage ($\Theta = 0.0625$) and metal surfaces, we used a structure with the symmetry of the substrate. This is because to the best of our knowledge, a detailed information as reported for Cu and Au in references [3] and [6] is still scarce in literature for Ag single crystals.

The adsorption energies are calculated on two single crystal surfaces considering top mono-dentate coordinations between O and Ag (surface atom) as initial geometry. The nature of the charge transfer process is analyzed by means of Mulliken population analysis to evaluate the atomic charges. All the calculations were performed with spin polarization (sp) and van der Waals interactions. Core electrons were

Table 1
Calculated concentrations of the phosphate species.

Solutions	pH	$[H_3PO_4]$	$[H_2PO_4^-]$	$[HPO_4^{2-}]$	$[PO_4^{-3}]$	$[H^+]$	$[OH^-]$
0.05 M K_3PO_4	12.56	5.63×10^{-18}	1.86×10^{-7}	0.03624	0.01375	2.759×10^{-13}	0.03624
0.01 M K_3PO_4	11.96	2.24×10^{-15}	1.86×10^{-7}	0.00912	0.00088	1.096×10^{-12}	0.00912
0.1 M KH_2PO_4	4.67	2.31×10^{-4}	0.099	2.52×10^{-4}	1.25×10^{-12}	2.12×10^{-5}	4.72×10^{-10}
0.01 M KH_2PO_4	4.79	1.75×10^{-5}	0.0099	3.34×10^{-5}	2.18×10^{-13}	1.60×10^{-5}	6.25×10^{-10}
0.1 M H_3PO_4	1.52	0.077	0.023	4.17×10^{-8}	1.46×10^{-19}	0.030	3.32×10^{-13}

replaced by norm-conserving pseudopotentials, built with the Troullier-Martins recipe [40] to represent the nucleus and the core electrons of the species considered. In the pseudopotential description of the atoms, only electronic valence states were considered. The basis set used for expanding in eigenstates was composed of double-polarized numerical orbitals (NAOs), which were solutions of the Kohn-Sham Hamiltonian for isolated pseudo-atoms. Exchange and correlation effects were described in the generalized gradient approximation (GGA) with Perdew-Burke-Ernzerhof (PBE) functional [41]. The energy of confinement (Energy-Shift) was 50 meV, which was the optimum value to obtain the best accuracy and computational efficiency for these systems. The energy cut-off (Mesh-Cut-Off) used was 150 Ry. The C6 coefficient in eV $Å^6$ used were: Ag: 155.13, H: 1.21, O: 6.08, and P: 67.74 and the van der Waals radii in Å were: Ag: 1.57, H: 1.00, O: 1.34, and P: 1.71 [42–44]. The minimum-energy configuration was determined by the conjugate gradient technique, which minimizes the system energy from an initial configuration with respect to the atomic coordinate until the force on each atom was less than 0.04 eV $Å^{-1}$. The minimum energy path (MEP) was optimized by means of the nudged elastic band method (NEB) [45,46].

3. Results

3.1. Cyclic voltammetry measurements

The predominant phosphate species present in K_3PO_4 aqueous electrolyte are PO_4^{3-} and HPO_4^{2-}, with a high concentration of the OH^- anion as shown in Table 1. Lucas et al. [47] reported surface oxidation in 0.1 M KOH at more positive potentials than −0.1 V vs. SCE, thus we took special care not to measure in that potential region [48–51].

Fig. 1 (upper panel) depicts *j–V* profiles of Ag(111) and Ag(100) electrodes in 0.05 M K_3PO_4 at 0.050 V s^{-1}. When the potential was scanned from negative to positive values, two anodic peaks were observed for both single crystal surfaces (V_p at −1.095 V and −0.59 V for Ag(100), and −1.060 V and −0.57 V for Ag(111)). For cathodic currents, there was a shoulder at −0.80 V on both single crystal surfaces, and well defined peaks were recorded at −0.98 and −0.99 V for Ag (111) and Ag(100), respectively. V_p values are slightly shifted towards more negative potentials for the (100) face.

Fig. 1 (lower panel) shows the *j–V* profiles of Ag(111) electrode in 0.01 M K_3PO_4 and 0.01 M KOH at 0.05 V/s. The effect of co-adsorption of hydroxide ions can be better appreciated from these profiles compared to upper panel figure. When only the hydroxide species is present in solution (dotted line), the features observed from −0.8 V to −0.4 V have been assigned to adsorption and structuration of the adsorbed layer [47]. The current starts increasing at potentials more negative than the *pzc* (≈ − 0.75 V), whereas at the phosphate solution (black circles) an analogous process starts at more negative potentials (shifted by 85 mV). Then, an anodic peak is observed at −0.55 V, where the corresponding cathodic peak was observed at −0.9 V (a peak separation of almost 400 mV). The inset of Fig. 1 lower panel shows the *j–V* profiles of Ag(111) and Ag(100) in 0.01 M KOH. These voltammetric responses are in agreement with in-situ and classical electrochemical measurements [47,49,51].

Lucas et al. [47] described the structure of Ag(111)/0.1 M KOH interface by means of Surface X-ray Scattering measurements (SXS). They observed an $OH_{(ads)}$ ordered layer with a coverage of 0.35, where the distance of K^+ ions to the Ag(111) surface depends on the electrode potential. Jovic et al. [49] reported the formation of a reversible ordered $OH_{(ads)}$ monolayer, where OH^- was adsorbed during the anodic scan and desorbed in the cathodic scan. We observed an analogous process when the *j–V* profiles of Ag(111) electrode were recorded in 0.01 M K_3PO_4 (Fig. 1 lower panel, black circles). The current starts increasing at more negative potentials than the *j–V* profiles in 0.01 M KOH, which can be attributed to the onset of hydroxide adsorption in the presence of the adsorbed phosphate species [14]. The anodic peak

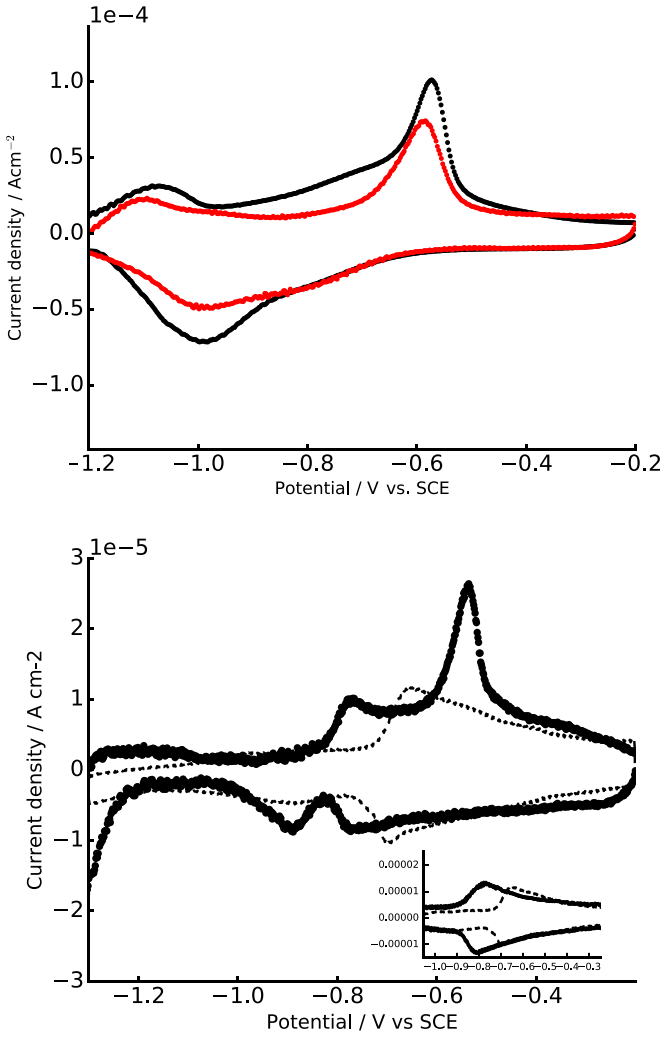

Fig. 1. Upper panel: Current density vs. potential (*j–V*) profiles of the Ag(111) (black) and Ag(100) (red) electrodes in 0.05 M K_3PO_4. Scan rate 0.050 V s^{-1}. Lower panel: *j–V* profiles of the Ag(111) electrode in 0.01 M K_3PO_4 (black circles) and 0.01 M KOH (dotted line). Inset: *j–V* profiles of the Ag(111) (dotted line) and Ag(100) (solid line) electrodes in 0.01 M KOH. Scan rate 0.050 V s^{-1}. (For interpretation of the references to color in this figure legend, the reader is referred to the web version of this article.)

observed at −0.55 V, can be associated to the formation and/or restructuring of the phosphate adsorbed layer [10,14,52]. The surface coordination of the phosphate species can be induced to change from bi-dentate to tri-dentate when scanning towards more positive potentials, and as the potential was scanned up to −0.2 V, the oxide was not formed. Niaura et al. [10] studied the adsorption of phosphate species on silver, gold, and copper electrodes by SERS. They proposed monodentate surface coordination of the PO_4^{-3} and HPO_4^{2-} ions and interpreted the dependence of the relative intensity of the internal modes on electrode potential in terms of the migration of P–O groups from the surface, as potential became more negative. The co-adsorption of hydroxide ions increased as the potential was scanned towards more positive values and the formation of surface oxides was not detected. For the strength of phosphate adsorption the following order was estimated: Cu > Au > Ag.

Fig. 2 shows current density peaks vs. scan rate (ν) of Ag(111) (upper left) and Ag(100) (upper right) electrodes in 0.05 M K_3PO_4 (cathodic $|\Delta j_{p_c}|$ black circles, and anodic $|\Delta j_{p_a}|$, red circles). The potential scan was started from the most negative values. The 111 surface shows a different dependence of $|\Delta j_p|$ on ν with respect to the 100 surface. When the $[HPO_4^{2-}/PO_4^{3-}]$ ratio was about 10 (Table 1), competition for the adsorption sites between hydroxide and phosphate

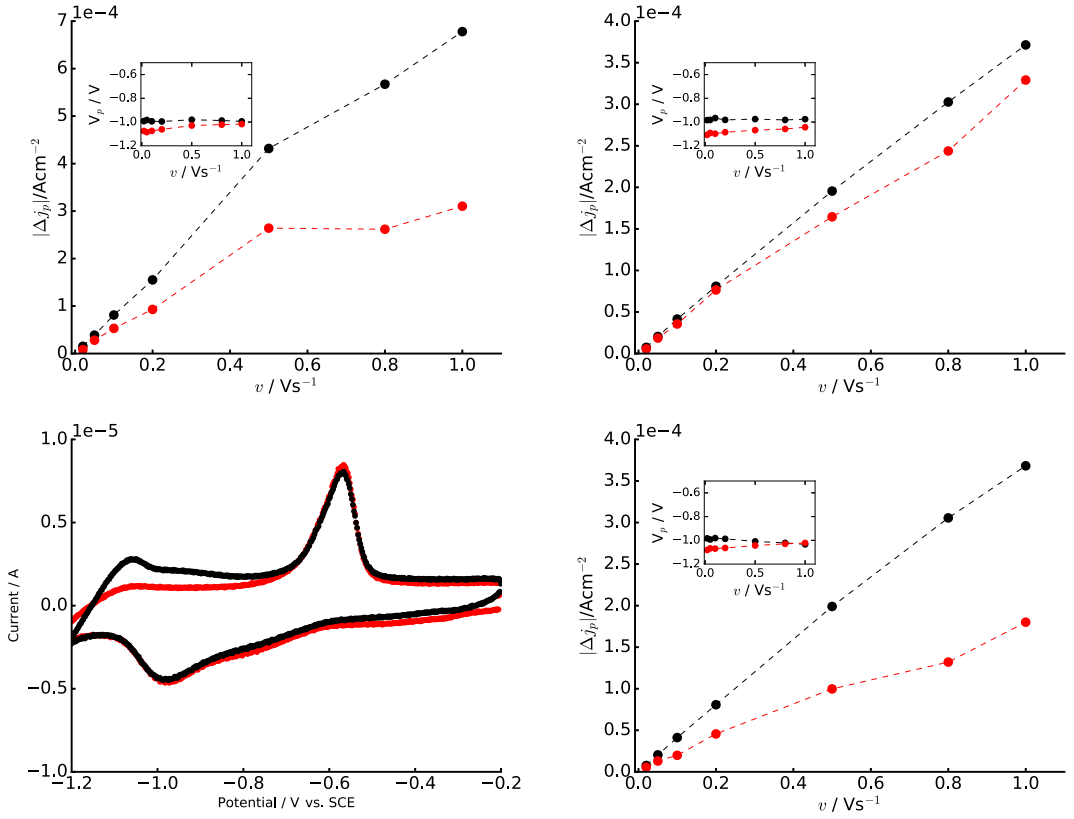

Fig. 2. Upper left panel: Peak current ($|\Delta j_p|$) vs. scan rate (v) of Ag(111) electrode in 0.05 M K_3PO_4. **Upper right panel**: $|\Delta j_p|$ vs. v of Ag(100) electrode in 0.05 M K_3PO_4. **Lower right panel**: $|\Delta j_p|$ vs. v of Ag(100) electrode in 0.01 M K_3PO_4. **Lower left panel**: j–V profiles of Ag(100) electrode in 0.01 M K_3PO_4. The potential scan was started from negative (black) towards more positive potential values, and from positive (red) towards more negative values. (For interpretation of the references to color in this figure legend, the reader is referred to the web version of this article.)

anions was stronger than at a lower ratio. Neither hydroxide nor phosphate species are adsorbed on the surface when the potential scan starts at −1.35 V [14,47,52]. Niaura et al. [14] have studied the effect of alkali metal cations on the surface-enhanced Raman spectra of phosphate anions adsorbed at silver electrodes, and they have demonstrated that phosphate species were not adsorbed at −1.4 V vs. Ag/AgCl(sat. KCl). The j–V profile obtained from −1.35 V (lower left panel, black circles) was different from that starting at −0.2 V (red circles), mainly in the anodic scan. The first anodic peak can be associated to the adsorption of phosphate species, and the second anodic peak to the formation/restructuring of the phosphate layer. Thus, the differences observed in the j–V profiles, when starting at −1.35 and at −0.2 V, can be explained by the absence and presence of an adsorbed phosphate layer, respectively. At 0.01 M K_3PO_4 the processes are better resolved (see Fig. 1 lower panel) than at 0.05 M, where the higher interaction between adsorbate-adsorbate and adsorbate-surface, mainly due to a higher coverage, may prevent a better differentiation between the processes.

Fig. 3 depicts the j–V profiles of Ag(111) and Ag(100) in 0.1 M KH_2PO_4 (upper panel) at 1.0 V s^{-1}. Bonding of the hydrogen ions to PO_4^{-3} results in reduced symmetry in $H_2PO_4^-$ ion, thus changing the features observed in the j–V profiles. Two cathodic peaks are observed at −0.46 V and −0.69 V for Ag(111), and at −0.67 V and −0.86 V for Ag(100). The separation in potential of cathodic/anodic peaks indicates quasi-reversible reactions for both electrode surfaces. Much research about adsorption of $H_2PO_4^-$ species on single crystals can be found in the literature, employing different techniques [4,5,11]. Weber et al. studied the adsorption of $H_2PO_4^-$ ion on Pt(111) in 10^{-3} M KH_2PO_4, observing a reversible process at −0.5 V vs. SHE. They also studied the adsorption of $H_2PO_4^-$ on Au(111) and Au(110) electrodes and no differences between the two surface orientations were reported, attributing these results to the fact that the $H_2PO_4^-$ has only two free oxygen atoms to coordinate to the electrode surface [12]. In this case, the proposed structure of the adsorbed ion was the two-fold through the two oxygen atoms. Our results show that the adsorption of $H_2PO_4^-$ ion on silver single crystals is stronger on Ag(100) electrodes. This behavior marks the strongest difference to the gold surfaces. Fig. 3 (lower panel) shows the j–V profiles of Ag(111) and Ag(100) electrodes in 0.10 M H_3PO_4 at 1 V s^{-1}. In this case, the differences between the 111 and 100 surfaces are more evident. The j–V profile for the 100 surface could not be recorded at values more negative than −0.7 V, due to the hydrogen evolution reaction.

Fig. 4 shows the cathodic and anodic $|\Delta j_p|$ responses as a function of scan rate for Ag(111) and Ag(100) electrodes in KH_2PO_4 solutions. A clearly different behavior can be observed when the KH_2PO_4 concentration in solution changes from 0.010 M to 0.10 M. Fig. 4 upper left and upper right panels show a linear dependence of $|\Delta j_p|$ on v, and the same slope for cathodic and anodic processes. The insets show the V_p dependence on v. From both ($|\Delta j_p|$ and V_p dependence on v) it can be inferred that the cathodic process is directly correlated to the anodic process on both electrodes, where the observation of a linear dependence on v, means that a process taking place on the electrode surface is detected.

At higher concentration of KH_2PO_4 (Fig. 4, lower left and lower right panels), two peaks can be clearly detected which display characteristic slopes, and their dependence on v is different for the two electrode surface orientations. For the Ag(111) electrode (Fig. 4 lower left panel), the $|\Delta j_p|$ of the anodic process tends to a saturation with increasing scan rate, while a linear behavior is observed for the cathodic process in the whole scan rate range. The opposite behavior is observed for Ag(100) electrodes, where the $|\Delta j_p|$ of the cathodic process shows saturation from 0.500 V s^{-1} for both peaks (Fig. 4 lower

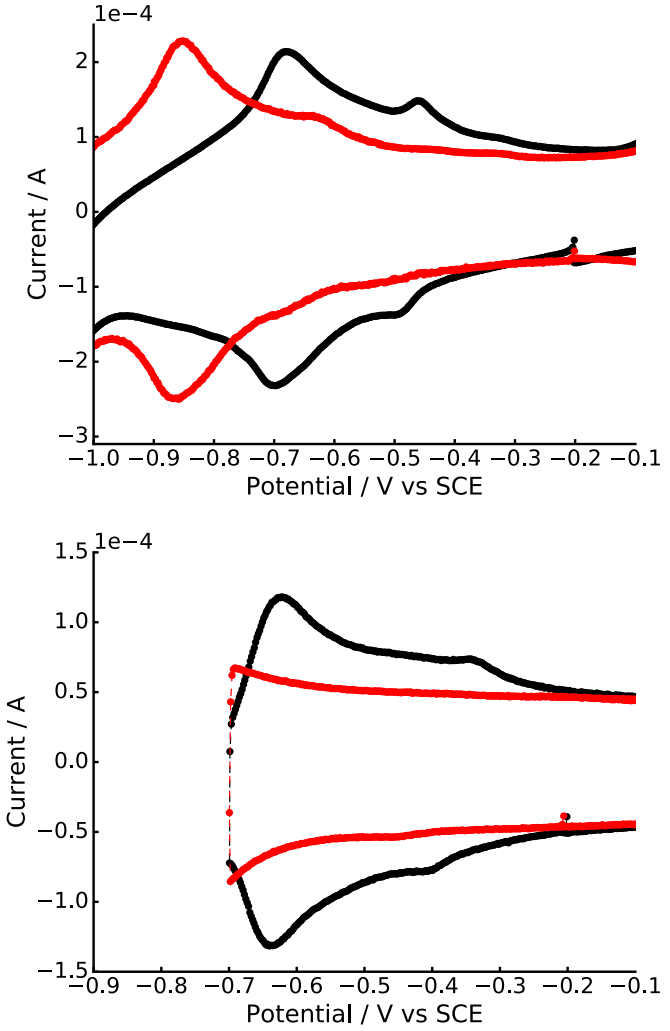

Fig. 3. *j–V* profiles of Ag(111) (black) and Ag(100) (red) electrodes in 0.1 M KH_2PO_4 (upper panel) and in 0.1 M H_3PO_4 (lower panel). The y-axis were multiply by a factor. Scan rate 1.0 V s^{-1}. (For interpretation of the references to color in this figure legend, the reader is referred to the web version of this article.)

right panel). The peak potential of the cathodic (V_{pc})/anodic (V_{pa}) processes occurring on Ag(100) surface (inset of Fig. 4 lower right panel) has almost the same value and remains constant for all investigated *v*. The changes observed in V_p values are noticeable for the Ag(111) surface (inset of Fig. 4 lower left panel). For the process occurring at more negative potential values, a 0.050 V of cathodic to anodic peak potential separation is observed. The processes occurring at more positive potential values (green and blue circles) showed a greater separation of almost 0.150 V.

Fig. 5 compares normalized current for *j–V* profiles of Ag(111) electrodes in 0.01 M K_3PO_4, KH_2PO_4 and H_3PO_4. It shows the potential shift for the different phosphate species, where a characteristic V_{pc} is displaced to more negative potential values as the negative charge on the species increases. For the three species, the order in which the cathodic peaks appear and the separation between them follow the same trend observed for theoretical results (see Table 2). The V_{pa} corresponding to the H_3PO_4 species was slightly more positive (by 0.060 V) than that corresponding to $H_2PO_4^-$ species. In the case of K_3PO_4, the separation in V_{pc}/V_{pa} values was about 0.260 V. During the cathodic scan, OH^- interference disappeared, due to OH^- desorption beginning before the phosphate. The more negative the cathodic V_{pc}, the higher the interaction between phosphate species and electrode surface.

Thus, cathodic peak potentials (V_{pc}^{111}) appear in the following order:

$$V_{pc}^{111}(PO_4^{3-}),\ (HPO_4^{2-}) < V_{pc}^{111}(H_2PO_4^-) < V_{pc}^{111}(H_3PO_4). \quad (1)$$

3.1.1. Current transient measurements

The initial potential was −0.40 V, condition which was maintained until a time-independent signal was recorded. A cathodic current was observed for all adsorbates, indicating that a given charge is taken from the electrode surface. These results can be correlated with the results obtained from theoretical computations. The current transient measurements where performed for all the systems investigated. Fig. 6 shows the current density as a function of time for a potential step applied to Ag(111) electrode in 0.01 M K_3PO_4. When starting from a steady state condition at −0.40 V, then changing the potential at −1.35 V during 600 s and finally returning to the initial potential value during 300 s, a higher cathodic current density during the potential pulse was observed. The steady state condition was restored within 450 s. After the current transient, the final state was recorded at −0.40 V, which was almost instantaneously established. The same behavior was observed for a V_{trans} of −0.40 V, when starting from −1.35 V. This demonstrates that under our experimental conditions, the electrode surface can be recovered with the same properties after pulses of different potential values are applied. At −0.4 V, PO_4^{3-}, HPO_4^{2-} and OH^- ions are competing by the surface adsorption sites, whereas at −1.35 V, all of them are desorbed.

3.2. Theoretical results

The adsorption of H_3PO_4, $H_2PO_4^-$ and PO_4^{3-} species on Ag(111) and Ag(100) was studied by means of DFT calculation. Fig. 7 shows – according to the size of the substrate employed and taking into account the periodic boundary conditions – the adsorbed species, which corresponds to ordered layers of p(4 × 4) structure. As previously mentioned, a low coverage was selected in order to achieve a better comparison between the different phosphate species. In both cases the film has the symmetry of the single crystal surface, i.e. C_{3v} and C_{4v} for adsorption on Ag(111) and Ag(100), respectively. In Fig. 8, the initial configuration of $H_2PO_4^-$ corresponds to mono-dentate binding species on a top site of the Ag(100) surface. The change in energies (Δ*E*[eV]) as a function of the Conjugate Gradient steps shows a monotonous decreasing change leading to bi-dentate adsorption. There is no barrier on the potential energy surface from the mono-dentate to bi-dentate position and the molecule change freely. There is a barrier of 0.37 eV from the bi-dentate to the tri-dentate position, which was calculated by means of nudged elastic band method (NEB). The tri-dentate position is the preferential configuration (0.65 eV more stable than the bi-dentate). The E_{ads} was determined as follows:

$$E_{ads}^{(hkl)} = E_{A/S(hkl)} - E_A - E_{S(hkl)} \quad (2)$$

where $E_{A/S(hkl)}$ denotes the phosphate species adsorbed on the surface; E_A is the phosphate species represented as a radical and $E_{S(hkl)}$ is the substrate in the vacuum.

Table 2 shows the E_{ads} calculated for the different species on Ag (111) and Ag(100) surfaces.

In all cases, the species are negatively charged (Q_{total}), except for phosphoric acid on Ag(111)

$$Q_{total} = \sum_{i=1}^{n} q_i \quad (3)$$

where Q_{total} is the sum of the atomic Mulliken charge of the atoms composing the species. The surface charge (Q_{sup}), is what the metal developed as a consequence of the adsorption process. It is of opposite sign to the species due to the charge transfer process.

$$Q_{sup} = -\frac{Q_{total}}{S} \quad (4)$$

where S is the surface area of the substrate. The Q_{total} values evidence

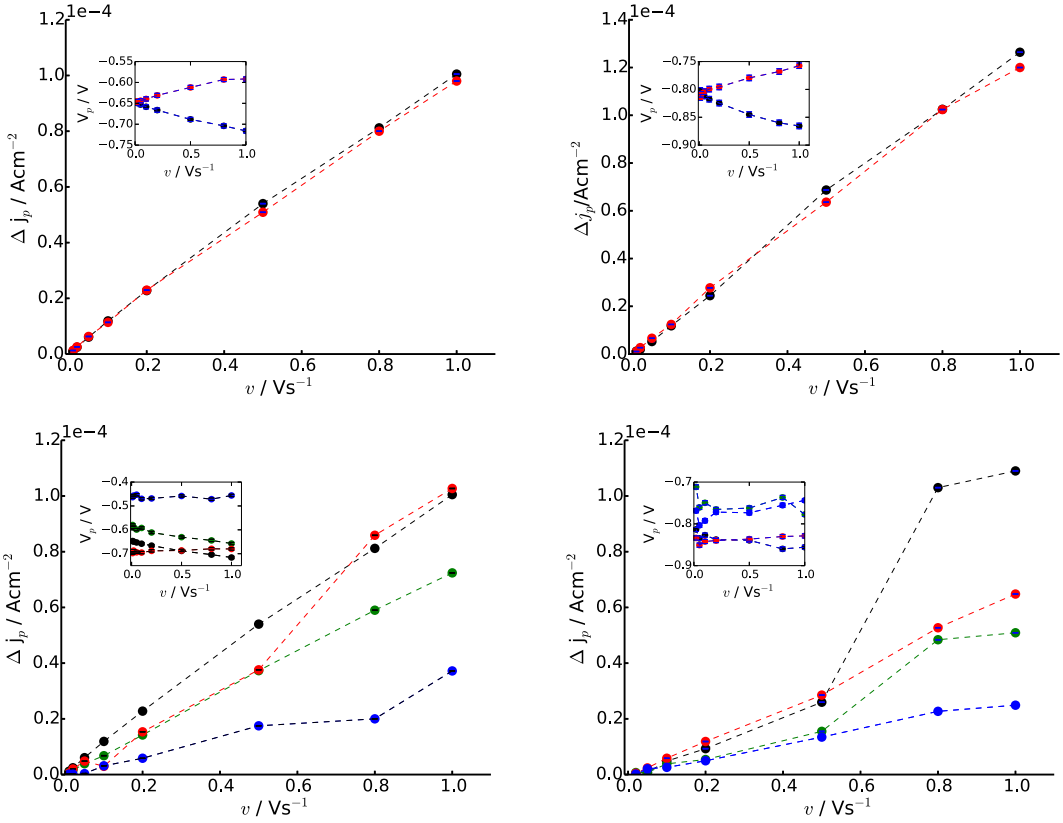

Fig. 4. $|\Delta j_p|$ vs. ν for KH_2PO_4 electrolyte in contact with Ag(111) and Ag(100) single crystal surfaces.Upper left panel: $|\Delta j_p|$ vs. ν for 0.01 M KH_2PO_4/Ag(111). Inset: Peak potential (V_p) vs. ν at −0.65 V vs. SCE; cathodic (**black**) and anodic (red). Upper right panel: $|\Delta j_p|$ vs. ν for 0.01 M KH_2PO_4/Ag(100). Inset: Peak potential (V_p) vs. ν at −0.80 V vs. SCE; cathodic (**black**) and anodic (red). Lower left panel: $|\Delta j_p|$ vs. ν for 0.1 M KH_2PO_4/Ag(111). Inset: Peak potential (V_p) vs. ν for peaks arising at −0.60 V and −0.65 V vs. SCE (cathodics: green and **black**); and at −0.70 V and −0.45 V vs. SCE (anodics: red and blue). Lower right panel: $|\Delta j_p|$ vs. ν for 0.1 M KH_2PO_4/Ag(100). Inset: Peak potential (V_p) vs. ν for peaks arising at −0.70 V and −0.80 V vs. SCE (cathodics: green and **black**); and at −0.85 V and −0.75 V vs. SCE (anodics: red and blue). The y-axes are multiplied by 1×10^{-4}.

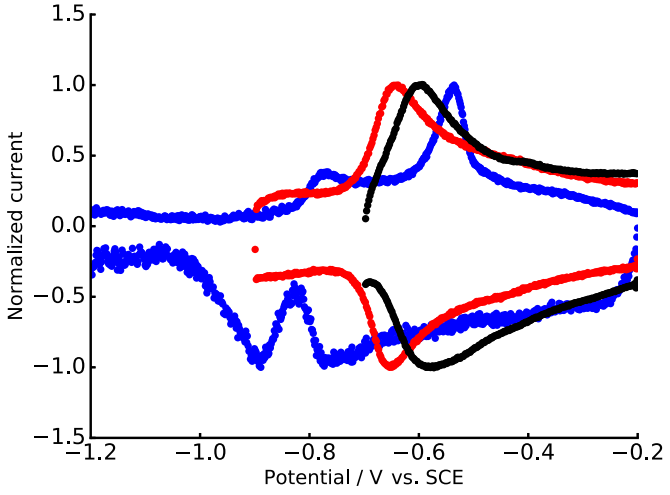

Fig. 5. Normalized *j–V* profiles of Ag(111) electrodes in 0.01 M K_3PO_4 (blue), KH_2PO_4 (red) and H_3PO_4 (black), in the −1.2 V to −0.2 V vs. SCE range. Scan rate 0.050 V s^{-1}. (For interpretation of the references to color in this figure legend, the reader is referred to the web version of this article.)

the formation of ordered structures, due to repulsive lateral interactions.

The P atomic charge (Q_p) decreases as the charge on phosphate species increases. When viewing the geometries, it can be seen that the tetrahedral structure of the phosphate species is compressed. This effect can be observed through the distance between the P atom and the surface (d_{P-sup}, Table 2). These trends observed in the structure, are related to the E_{ads} as shown below:

Table 2
Phosphate species at Θ = 0.0625 in a p(4 × 4) ordered layer adsorbed on Ag(111) and Ag (100). The adsorption energies E_{ads} are in eV, the phosphate-surface distances (d_{P-sup}) are in Å, Q_P (phosphorus atom charge) and Q_{total} (total charge of the species). Mulliken's charges are in atomic units (a.u.) and the surface charges are in C cm^{-2}.

Adsorbate	E_{ads}	d_{P-sup}	Q_P	Q_{total}	Q_{sup}
Ag(111)					
H_3PO_4	−1.08	3.20	0.23	1.08	-1.42×10^{-5}
$H_2PO_4^-$	−3.61	2.71	0.19	−0.55	7.25×10^{-6}
HPO_4^{2-}	−5.33	2.39	0.13	−1.05	1.38×10^{-5}
PO_4^{3-}	−6.11	2.36	0.08	−1.31	1.71×10^{-5}
Ag(100)					
H_3PO_4	−0.98	3.13	0.26	−0.19	2.63×10^{-6}
$H_2PO_4^-$	−3.71	2.83	0.22	−0.54	7.43×10^{-6}
HPO_4^{2-}	−5.78	2.39	0.16	−0.97	1.33×10^{-5}
PO_4^{3-}	−6.44	2.36	0.11	−1.31	1.79×10^{-5}

$$E_{ads}(PO_4^{3-}) < E_{ads}(HPO_4^{2-}) < E_{ads}(H_2PO_4^-) < E_{ads}(H_3PO_4). \quad (5)$$

In all cases, E_{ads} are of chemical type, within a range of −0.98 to −6.44 eV, which results in stable films of ordered structures on both single crystal surfaces. E_{ads} values for the different species follow the same trend observed in experimental results (Fig. 4 and Eq. (1)). Hydrogen loss in the phosphate species leads to a more stable structure on both surfaces.

In Fig. 9, we can note the change in E_{ads} for the different species through the Partial Density of States (PDOS) of the P atom adsorbed on Ag(111), which is the central atom of the oxoanion. While the atoms in contact with the surface are the three O atoms, it is not possible to compare the PDOS of all type of oxygen atoms, since it would involve

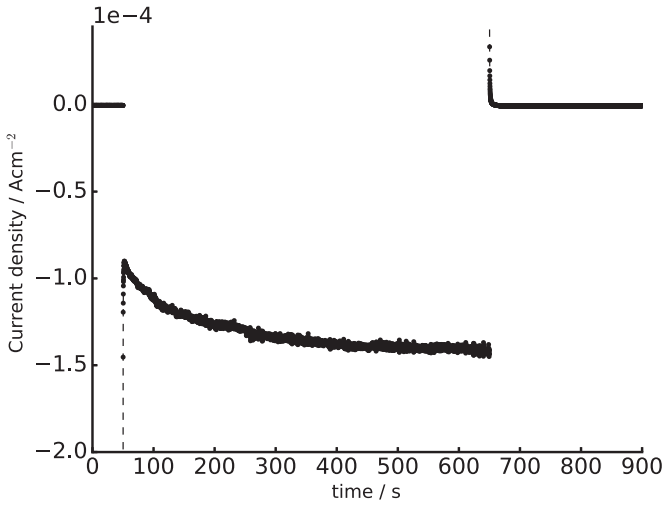

Fig. 6. Current density vs. time profiles of Ag(111) electrodes in 0.01 M K_3PO_4. Initial potential (V_i) −0.40 V vs. SCE. Potential step (V_{trans}) −1.35 V vs. SCE and Final potential (V_f) = V_i.

too much information which would make it difficult to draw conclusions. However, we can observe the changes in the intensity of electronic density of the orbitals involved in the bonds between the P with the four O atoms: 3s, $3p_x$, $3p_y$ and $3p_z$, which are related to the changes observed in the geometric structure of the oxoanions. There are changes in the angles and in the tetrahedral shape of the anionic species, which gets deformed, becomes more compressed and less high. All these effects can be observed through a change in the d_{P-sup}. The black line corresponds to H_3PO_4 species where the P atom is at a distance of 3.20 Å from the surface. The highest band of the total density appeared between −10.5 and −9.5 eV because of the interaction of the 3p orbitals with the 5s band of the silver surface. The more deprotonated the phosphate species, $H_2PO_4^-$ (red line) and PO_4^{3-} (blue line) are, the P atom becomes closer to the surface (2.71 and 2.36 Å, respectively), and the species develop negative charges of −0.55 and −1.31 eV, respectively. These charges produce a shift of the bands to higher energies. Since the P atom is close to the surface, the 3s and 3pz orbitals interacted with the 4d bands of the metal surface, which appear in the region of −6 to −2 eV.

Fig. 10 shows the PDOS vs. energy plot corresponding to P atom of the phosphate species adsorbed on Ag(100). Changes of the PDOS profiles were produced by changing the single crystal surface. Although the orbitals 3s and 3p of the P atom exhibit qualitatively the same changes as in the Ag(111), the magnitude of the displacements and the intensity of the peaks, were modified due to the new crystallographic

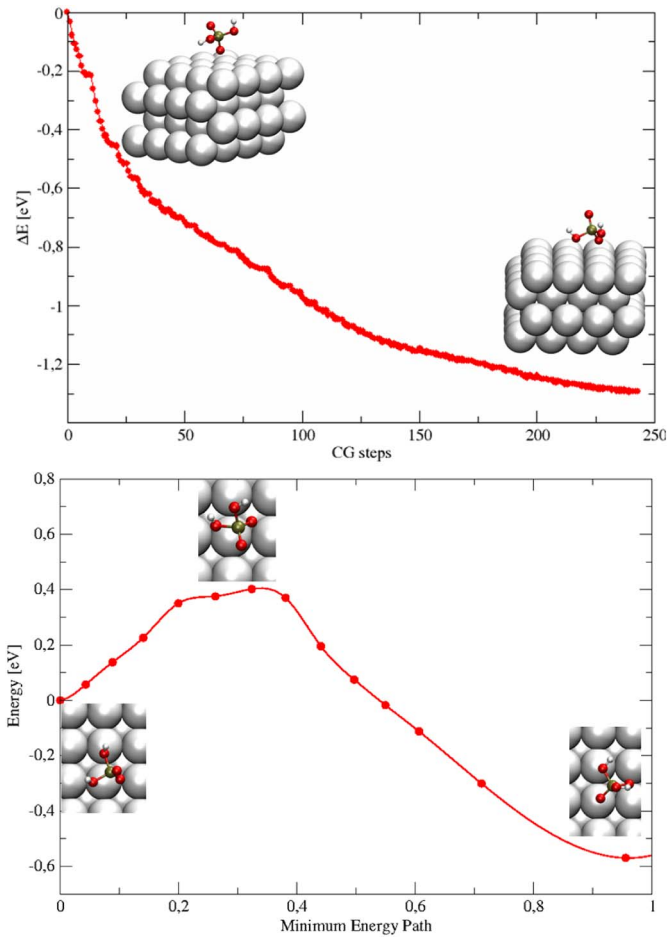

Fig. 8. CG energy changes [eV] vs minimization from the mono-dentate to bi-dentate adsorption position of $H_2PO_4^-$ on Ag(100) (upper panel). Minimum Energy Path for the bi-dentate to tri-dentate change of position (lower panel).

order of the substrate. The main differences on the total profiles were observed between −10.5 and −6 eV.

As a first approach in these DFT calculations, the presence of the solvent was not taken into account. However, the fact that the trends of the experimental results were qualitatively reproduced by the calculations, suggests that the adsorption phenomenon was mainly dominated by the adsorbate/substrate interaction. The trends observed for both crystallographic orientations were in agreement with the experimental results measured at macroscopic level.

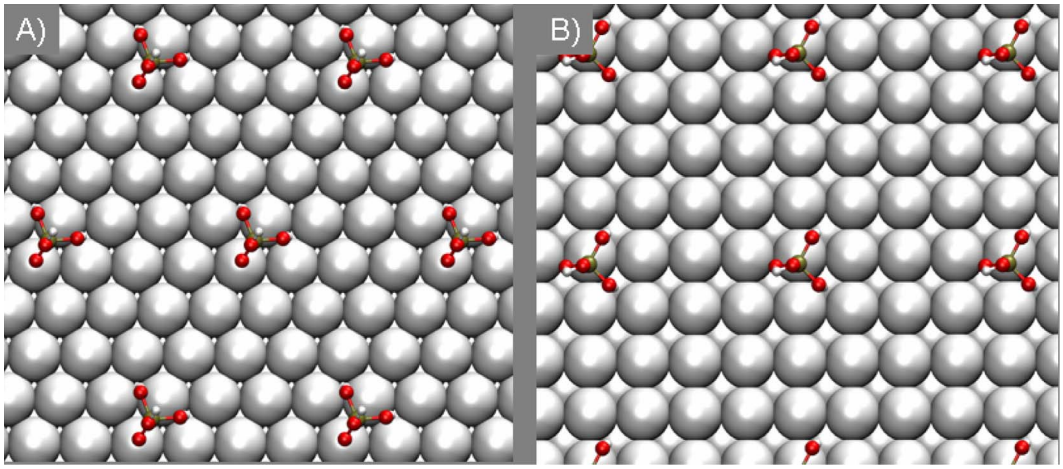

Fig. 7. Optimized geometry of the H_3PO_4 molecule forming a p(4 × 4) structure on A) Ag(111) and B) Ag(100).

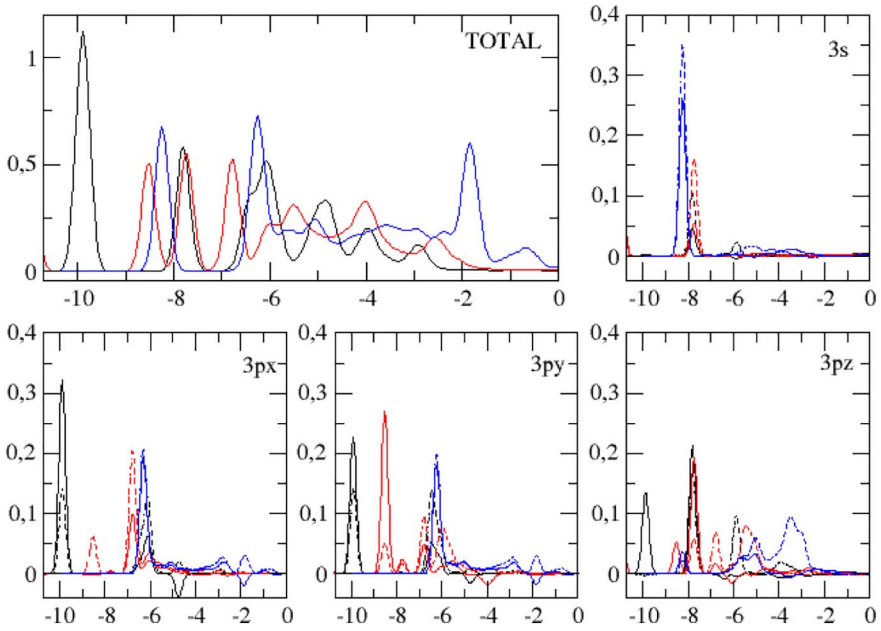

Fig. 9. PDOS vs. energy for the P atom adsorbed on Ag(111). Black: H_3PO_4, red: $H_2PO_4^-$ and blue: PO_4^{3-}. Solid line: spin up; dashed line: spin down. The zero energy corresponds to the Fermi energy level. (For interpretation of the references to color in this figure legend, the reader is referred to the web version of this article.)

4. Discussion

The identity of the predominantly adsorbed anion strongly depends on the electrode potential. The changes in the symmetry of the adsorbed phosphate species as a function of potential are related to the *pztc* of the electrode [10]. The phosphate species adsorbed on silver electrodes as a function of applied potential has been studied by SERS [14,52]. It has been determined that at more negative potentials (−0.8 V vs. Ag/AgCl(sat KCl)), the P–O–M mode transforms into P–O–H (the solvent exposed P–O bands) due to its high sensitivity to hydrogen-deuterium exchange experiments [14]. The potential-dependent conformational geometry of the adsorbed phosphate, and a surface free of adsorbed anions at −1.4 V was demonstrated by these authors. Avalle et al. [32] studied the Ag(111) electrode in 0.010 M $KClO_4$ and observed that the shape and position of the current density peaks in the CV profiles changes upon injection of analytes (which differ only in the phosphate moiety), indicating a strong interaction between these ions and the Ag(111) surface. It has been proven that, for silver electrodes, the applied potential is the main factor that controls the interaction between the metal surface and the adsorbates [14,32,52,53]. Jovic et al. [49] studied the hydroxide adsorption on Ag(100) and Ag(111) electrodes at two different concentrations of NaOH, and proposed a complete charge transfer between this ion and the electrodes. As a result of the oxidation/reduction of the Ag_2O a roughening of the silver surface was observed.

Experimental studies of phosphate species adsorption performed on gold and platinum single crystal electrodes in solutions containing HF/KF as supporting electrolyte [9,11], reveal a dependence of the nature and/or geometry of the adsorbed phosphate species on both, the nature of the electrode and the applied potential. However, in the case of platinum electrodes, an absence of surface specificity regarding the geometric distribution of surface atoms was observed at the more positive adsorption potentials, under the given experimental conditions [7]. The changes in symmetry for the adsorbed phosphate species on Pt were assigned to the different dissociation of the anionic species upon adsorption, mainly due to the polyprotic nature of phosphoric

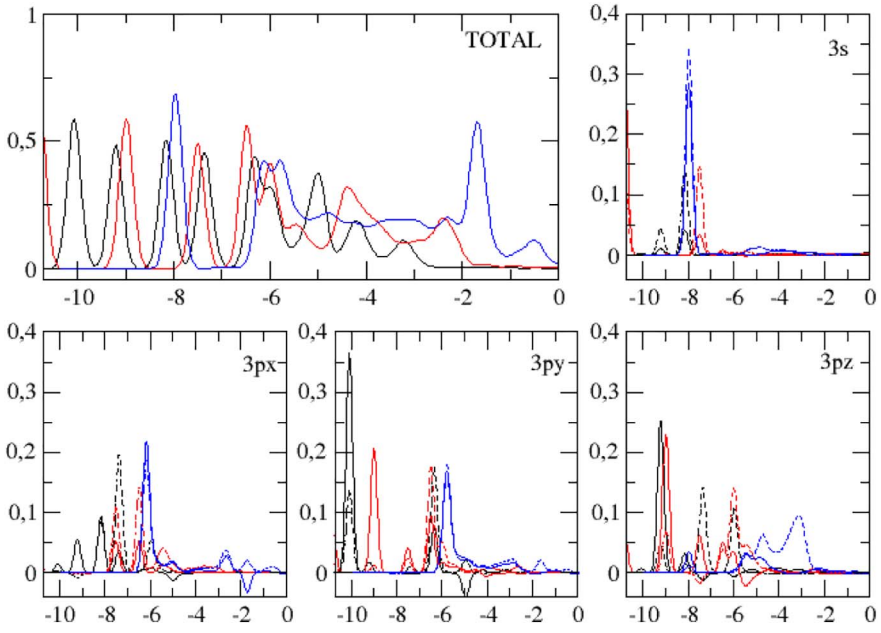

Fig. 10. PDOS vs. energy for the P atom adsorbed on Ag(100). Black: H_3PO_4, red: $H_2PO_4^-$ and blue: PO_4^{3-}. Solid line: spin up; dashed line: spin down. The zero energy corresponds to the Fermi energy level. (For interpretation of the references to color in this figure legend, the reader is referred to the web version of this article.)

acid [5,11]. The phosphate species adsorbed on Au(111) electrodes did not show any symmetry changes even for high positive potentials [33]. Other remarkable fact observed for Au(100) electrodes, was that the presence of adsorbed phosphate species shifts the lifting of surface reconstruction to lower potentials by 0.20 V.

Weber et al. [12] studied the adsorption of $H_2PO_4^-$ on Au(100) and Au(111) by in situ Fourier Transform Infrared Spectroscopy (FTIS). They observed that the structure of the phosphate species adsorbed on both electrodes presents the same characteristics. They concluded that this was not an unexpected result since $H_2PO_4^-$ ions have only two oxygen atoms free to coordinate to the surface (thus, the crystallographic structure of the electrode does not determine the structure of the adsorbed ion.). Then, the coordination of $H_2PO_4^-$ ion for both electrodes was two-fold through the two oxygen atoms. In our case, the shifting and change in shape of the peaks, indicate that the structure and chemical interactions are likely to be different for the two crystallographic orientations. The surface concentration can be considered as the result of contributions by the predominant species present in solution. In electrolytes containing phosphate anions, the following acid-base equilibrium hold as shown below:

$$H_3PO_{4(aq)} \rightleftarrows H^+_{(aq)} + H_2PO^-_{4(aq)} \quad pK_a = 2.04 \tag{6}$$

$$H_2PO^-_{4(aq)} \rightleftarrows H^+_{(aq)} + HPO^{2-}_{4(aq)} \quad pK_a = 7.27 \tag{7}$$

$$HPO^{2-}_{4(aq)} \rightleftarrows H^+_{(aq)} + PO^{3-}_{4(aq)} \quad pK_a = 12.98. \tag{8}$$

Considering the experimental and theoretical results for the particular case of Ag(100) electrodes in 0.010 M KH_2PO_4, where the HPO_4^{2-}/$H_2PO_4^-$ ratio in solution is 1/298 (i.e. the $H_2PO_4^-$ is the predominant ion, see Table 1), a tri-dentated coordination for the adsorbed species and the formation of an ordered layer are expected. A bi-dentated coordination is also possible but less stable. The rotation between these two coordinations is not possible due to to the fact that a high barrier must be overcome at room temperature. However, the change can occur through mechanisms involving participation of the solvent. From experiments, a reversible process was detected, which strongly depended on the surface crystallographic orientation and the initial concentration of the KH_2PO_4 solution.

In K_3PO_4, PO_4^{3-}, HPO_4^{2-} and OH^- species are simultaneously adsorbed at the electrode surface. It was demonstrated that their adsorption has a competitive character.

5. Conclusions

In the present work phosphate species adsorption on Ag(111) and Ag(100) was investigated by means of computational and experimental studies and the following conclusions were drawn:

- Adsorption of phosphate species on silver single crystals is highly sensitive to surface structure, in contrast to what was observed for gold single crystals.
- The V_{pc}^{hkl}(anion) depends on the crystallographic orientation of the electrode surface and the predominant species in solution. The following trends were observed:

  $V_{pc}^{111}(PO_4^{3-}, HPO_4^{2-}) < V_{pc}^{111}(H_2PO_4^-) < V_{pc}^{111}(H_3PO_4)$

  and

  $V_{pc}^{100}(PO_4^{3-}, HPO_4^{2-}) < V_{pc}^{100}(H_2PO_4^-)$.

  The $V_{pc}^{100}(H_3PO_4)$ was not observed within the potential range studied. Experimental results follow the same qualitative trends as theoretical ones.
- Due to OH^- co-adsorption in K_3PO_4, V_{pa}^{hkl}(anion) appears as follows:

  $V_{pa}^{hkl}(H_2PO_4^-) < V_{pa}^{hkl}(H_3PO_4) < V_{pa}^{hkl}(PO_4^{3-}, HPO_4^{2-})$.

- A stable phosphate species adlayer was formed at potentials higher than that of zero total charge (*pztc*) for Ag(111) and Ag(100) electrodes. In the particular case of Ag(100)/H_3PO_4, peaks were not observed from *j–V* profiles in the potential range studied.
- Complexity of the processes increased with hydrogen loss in phosphate molecules.
- We also studied the phosphate(ads)/Ag(111) and phosphate(ads)/Ag(100) interfaces by means of theoretical calculations to obtain accurate information at an atomic scale. We found that all phosphate films on silver are stable and have the same symmetry as the single crystal surface.
- As the anion charge increases (for the different species studied) so does film stability. The films formed have in all cases ordered structures due to the fact that charged anions cause repulsive lateral interactions.
- Theoretical results are consistent with the sensitivity observed in electrochemical measurements on Ag(111) and Ag(100) electrodes.

Acknowledgments

This work was supported by PIP 11220120100031 and 11220100100411 from CONICET. SECyT UNC, CCAD-UNC, and GPGPU Computing Group, Argentina, are also acknowledged. The authors also wish to thank language assistance by Ms. R.K. Plasencia.

References

[1] M.J.S. Farias, G.A.B. Mello, A.A. Tanaka, J.M. Feliu, J. Catal. 345 (2017) 216–227, http://dx.doi.org/10.1016/j.jcat.2016.11.031.
[2] M. Yaguchi, T. Uchida, K. Motobayashi, M. Osawa, J. Phys. Chem. Lett. 7 (2016) 3097–3102, http://dx.doi.org/10.1021/acs.jpclett.6b01342.
[3] C. Schlaup, S. Horch, Surf. Sci. 608 (2013) 44–54, http://dx.doi.org/10.1016/j.susc.2012.09.011.
[4] J. Mostany, P. Martínez, V. Climent, E. Herrero, J.M. Feliu, Electrochim. Acta 54 (2009) 5836–5843, http://dx.doi.org/10.1016/j.electacta.2009.05.040.
[5] R. Gisbert, G. García, M.T.M. Koper, Electrochim. Acta 55 (2010) 7961–7968, http://dx.doi.org/10.1016/j.electacta.2010.04.009.
[6] A. Cuesta, M. Kleinert, D.M. Kolb, Phys. Chem. Chem. Phys. 2 (2000) 5684–5690, http://dx.doi.org/10.1039/b006464p.
[7] S. Ye, H. Kita, A. Aramata, J. Electroanal. Chem. 333 (1992) 299–312, http://dx.doi.org/10.1016/0022-0728(92)80398-N.
[8] F.C. Nart, T. Iwasita, M. Weber, Ber. Bunsenges. Phys. Chem. 97 (5) (1993) 737–738, http://dx.doi.org/10.1002/bbpc.19930970515.
[9] M. Weber, F.C. Nart, Electrochim. Acta 41 (5) (1996) 653–659, http://dx.doi.org/10.1016/0013-4686(95)00353-3.
[10] G. Niaura, A.K. Gaigalas, V.L. Vilker, J. Phys. Chem. B 101 (1997) 9250–9262, http://dx.doi.org/10.1021/jp970097k.
[11] M. Weber, F.C. Nart, I.R. De Moraes, T. Iwasita, J. Phys. Chem. 100 (1996) 19933–19938, http://dx.doi.org/10.1021/jp960952k.
[12] M. Weber, I.R. de Moraes, A.J. Motheo, F.C. Nart, Colloids and Surfaces A: Physicochemical and Engineering Aspects 134 (1998) 103–111, http://dx.doi.org/10.1016/S0927-7757(97)00333-6.
[13] T. Fukuda, A. Aramata, J. Electroanal. Chem. 440 (1997) 153–161, http://dx.doi.org/10.1016/S0022-0728(97)80051-4.
[14] G. Niaura, R. Jakubėnas, J. Electroanal. Chem. 510 (2001) 50–58, http://dx.doi.org/10.1016/S0022-0728(01)00542-3.
[15] I.R. Moraes, F.C. Nart, J. Electroanal. Chem. 563 (1) (2004) 41–47, http://dx.doi.org/10.1016/j.jelechem.2003.08.018 (15).
[16] F. Silva, A. Martins, Electrochim. Acta 44 (6–7) (1998) 919–929, http://dx.doi.org/10.1016/S0013-4686(98)00195-9.
[17] F. Silva, A. Martins, J. Electroanal. Chem. 467 (1–2) (1999) 335–341, http://dx.doi.org/10.1016/S0022-0728(99)00165-5.
[18] Q. He, X. Yang, W. Chen, S. Mukerjee, B. Koel, S. Chen, Phys. Chem. Chem. Phys. 12 (2010) 12544–12555, http://dx.doi.org/10.1039/c0cp00433b.
[19] E.C. Le Ru, P.G. Etchegoin, Principles of Surface-Enhanced Raman Spectroscopy, Elsevier B.V., 978-0-444-52779-0, 2009.
[20] F. Tielens, C. Gervais, G. Deroy, M. Jaber, L. Stievano, C. Coelho Diogo, J.-F. Lambert, Langmuir 32 (4) (2016) 997–1008, http://dx.doi.org/10.1021/acs.langmuir.5b03519.
[21] J.F. Li, Y.F. Huang, Y. Ding, Z.L. Yang, S.B. Li, X.S. Zhou, F.R. Fan, W. Zhang, Z.Y. Zhou, D.Y. Wu, B. Ren, Z.L. Wang, Z.Q. Tian, Lett. Nat. 464 (2010) 392–395, http://dx.doi.org/10.1038/nature08907.
[22] J.-F. Li, Y.-J. Zhang, A.V. Rudnev, J.R. Anema, S.-B. Li, W.-J. Hong, P. Rajapandiyan, J. Lipkowski, T. Wandlowski, Z.-Q. Tian, J. Am. Chem. Soc. 137 (2015) 2400–2408, http://dx.doi.org/10.1021/ja513263j.
[23] U.K. Sur, J. Chowdhury, Curr. Sci. 105 (7) (2013) 923–939.
[24] J.-C. Dong, R. Panneerselvam, Y. Lin, X.-D. Tian, J.-F. Li, Adv. Opt. Mater. (2016)

1–15, http://dx.doi.org/10.1002/adom.201600223.
[25] A. Tanaka, R. Adzic, B. Nikolic, J. Serb. Chem. Soc. 64 (1999) 695–705.
[26] O.M. Magnussen, J. Hageböck, J. Holos, R.J. Behm, Faraday Discuss. 94 (1992) 329–338, http://dx.doi.org/10.1039/FD9929400329.
[27] X. Gao, G.J. Edens, F.C. Liu, A. Hamelin, M.J. Weaver, J. Phys. Chem. 98 (1994) 8086–8095, http://dx.doi.org/10.1021/j100084a027.
[28] O.M. Magnussen, B.M. Ocko, R.R. Adzic, J. Wang, Phys. Rev. B 51 (1995) 5510–5513, http://dx.doi.org/10.1103/PhysRevB.51.5510.
[29] M.L. Para, O.E. Linarez Pérez, M.I. Rojas, M. López Teijelo, J. Phys. Chem. C 120 (2016) 4364–4372, http://dx.doi.org/10.1021/acs.jpcc.5b11146.
[30] V. Stamenkovic, N.M. Markovic, P.N. Ross Jr, J. Electroanal. Chem. 500 (2001) 44–51, http://dx.doi.org/10.1016/S0022-0728(00)00352-1.
[31] S.L.J. Tan, J.M. Kan, R.D. Webster, J. Phys. Chem. B 117 (2013) 13755–13766, http://dx.doi.org/10.1021/jp4069619.
[32] L.B. Avalle, L. Valle, J. Electroanal. Chem. 662 (2011) 288–297, http://dx.doi.org/10.1016/j.jelechem.2011.07.020.
[33] Andrzej Wieckowski (Ed.), Interfacial Electrochemistry: Theory: Experiment, and Applications, Taylor & Francis, 1999.
[34] A.J. Bard, L.R. Faulkner, Electrochemical Methods: Fundamentals and Applications, John Wiley and Sons, Inc, 2001.
[35] E. Santos, L.B. Avalle, K. Pötting, P. Vélez, H. Jones, Electrochim. Acta 53 (2008) 6807–6817, http://dx.doi.org/10.1016/j.electacta.2007.12.080.
[36] A. Hamelin, L. Stoicoviciu, J. Electroanal. Chem. 271 (1989) 15–26, http://dx.doi.org/10.1016/0022-0728(89)80060-9.
[37] A. Ruderman, M.F. Juarez, G. Soldano, L.B. Avalle, G. Beltramo, M. Giesen, E. Santos, Electrochim. Acta 109 (2013) 403–410, http://dx.doi.org/10.1016/j.electacta.2013.07.112.
[38] E. Herrero, L.J. Buller, H.D. Abruña, Chem. Rev. 101 (2001) 1897–1930, http://dx.doi.org/10.1021/cr9600363.
[39] J.M. Soler, E. Artacho, J.D. Gale, A. García, J. Junquera, P. Ordejón, D. Sánchez-Portal, J. Phys. Condens. Matter 14 (2002) 2745–2779 (PII: S0953-8984(02)30737-9).
[40] N. Troullier, J.L. Martins, Phys. Rev. B: Condens. Matter Mater. Phys. 43 (1991) 1993–2006, http://dx.doi.org/10.1103/PhysRevB.43.1993.
[41] J.P. Perdew, K. Burke, M. Ernzerhof, Phys. Rev. Lett. 77 (1996) 3865–3868, http://dx.doi.org/10.1103/PhysRevLett.77.3865.
[42] S. Grimme, J. Comput. Chem. 27 (2006) 1787–1799, http://dx.doi.org/10.1002/jcc.20495.
[43] K. Tonigold, A. Groß, J. Chem. Phys. 132 (2010) 224701–224710, http://dx.doi.org/10.1063/1.3439691.
[44] F. Göltl, A. Grüneis, T. Bućko, J. Hafner, J. Chem. Phys. 137 (2012) 114111–114117, http://dx.doi.org/10.1063/1.4750979.
[45] G. Henkelman, B.P. Uberuaga, H. Jónsson, J. Chem. Phys. 113 (2000) 9901–9904, http://dx.doi.org/10.1063/1.1329672.
[46] G. Henkelman, H. Jónsson, J. Chem. Phys. 113 (2000) 9978–9985, http://dx.doi.org/10.1063/1.1323224.
[47] C.A. Lucas, P. Thompson, Y. Gründer, N.M. Markovic, Electrochem. Commun. 13 (2011) 1205–1208, http://dx.doi.org/10.1016/j.elecom.2011.08.043.
[48] M. López Teijelo, J.R. Vilche, A.J. Arvia, J. Appl. Electrochem. 18 (1988) 691–698, http://dx.doi.org/10.1007/BF01016894.
[49] B.M. Jovic, V.D. Jovic, G.R. Stafford, Electrochem. Commun. 1 (1999) 247–251, http://dx.doi.org/10.1016/S1388-2481(99)00049-1.
[50] S.L. Horswell, A.L.N. Pinheiro, E.R. Savinova, B. Pettinger, M.-S. Zei, G. Ertl, J. Phys. Chem. B 108 (2004) 18640–18649, http://dx.doi.org/10.1021/jp0481198.
[51] S.L. Horswell, A.L.N. Pinheiro, E.R. Savinova, M. Danckwerts, B. Pettinger, M.-S. Zei, G. Ertl, Langmuir 20 (2004) 10970–10981, http://dx.doi.org/10.1021/la0483818.
[52] P.B. Dorain, K.U. Von Raben, R.K. Chang, Surf. Sci. 148 (1984) 439–452, http://dx.doi.org/10.1016/0039-6028(84)90591-0.
[53] S.J. Greaves, W.P. Grifith, J. Ram, Spectroscopy 19 (1988) 503–507, http://dx.doi.org/10.1002/jrs.1250190803.